Relativistic coupled-cluster calculations of ^{20}Ne, ^{40}Ar, ^{84}Kr, and ^{129}Xe: Correlation energies and dipole polarizabilities

B. K. Mani,[1] K. V. P. Latha,[2] and D. Angom[1]
[1]*Physical Research Laboratory, Navarangpura, 380009 Gujarat, India*
[2]*Department of Electrophysics, National Chiao-Tung University, 1001 University Road, Hsinchu, Taiwan 300, Republic of China*
(Received 13 August 2009; published 4 December 2009)

We have carried out a detailed and systematic study of the correlation energies of inert gas atoms Ne, Ar, Kr, and Xe using relativistic many-body perturbation theory and relativistic coupled-cluster theory. In the relativistic coupled-cluster calculations, we implement perturbative triples and include these in the correlation energy calculations. We then calculate the dipole polarizability of the ground states using perturbed coupled-cluster theory.

DOI: 10.1103/PhysRevA.80.062505 PACS number(s): 31.15.bw, 31.15.ve, 31.15.ap, 31.15.am

I. INTRODUCTION

High precision atomic experiments are at the core of several investigations into fundamental physics and high end technology developments. Selected examples are search for electric dipole moment (EDM) [1] and observation of parity nonconservation [2]. These endeavors, in general, require precision atomic theory calculations to analyze the results and understand systematics. The challenging part of precision atomic structure and properties calculations is obtaining accurate wave functions. In the case of high Z atoms, the need to incorporate relativity adds to the difficulty. A systematic study of the correlation energy is one of the possible methods to test the accuracy of the atomic wave function. In this paper, we report the results of correlation energy calculations of inert gas atoms Ne, Ar, Kr, and Xe. For this we employ many-body perturbation theory (MBPT) and calculate the second-order correlation energy. A comparative study reveals the changing nature of electron correlations in the group. Our interest in particular is Xe, which is a candidate for EDM experiments [3] and theoretical calculations [4].

For completeness, in the presentation of the paper, we give an overview of MBPT. It is a powerful theory and forms the basis of other more sophisticated and elaborate many-body methods. However, one drawback of MBPT is the complexity of expressions at higher orders. This renders the theory inappropriate to incorporate strong correlation effects in heavy atoms. Yet, at lower orders its simplicity makes it an ideal choice to test and optimize basis sets. We use this insight to generate basis sets for coupled-cluster calculations.

The coupled-cluster theory, first developed in nuclear many body physics [5,6], is considered the most accurate many body theory. In recent times, it has been used with great success in nuclear [7], atomic [8,9], molecular [10], and condensed matter [11] calculations. It is equivalent to incorporating electron correlation effects to all orders in perturbation. The theory has been used in performing high precision calculations to study the atomic structure and properties. These include atomic electric dipole moments [8,12], parity nonconservation [13], hyperfine structure constants [9,14], and electromagnetic transition properties [15,16]. In the present work we use the relativistic coupled-cluster singles and doubles (CCSD) approximation to calculate correlation energy and dipole polarizability of inert gas atoms Ne, Ar, Kr, and Xe. In the dipole polarizability calculations, the dipole interaction Hamiltonian is introduced as a perturbation. A modified theory, recently developed [17], incorporates the perturbation within the coupled-cluster theory. This theory has the advantage of subsuming correlation effects more accurately. The results provide a stringent test on the quality of the wave functions as the dipole polarizability of inert gas atoms are known to high accuracy [18]. Based on the CCSD method, we also estimate the third-order correlation energy. Further more, perturbative triples are incorporated in the coupled-cluster calculations.

In the paper we give a brief description of MBPT in Sec. II and discuss the method to calculate electron correlation energy to the second and third order in residual Coulomb interaction. The coupled-cluster theory is described in Sec. III, where we also discuss linearized coupled-cluster theory and correlation energy calculation using coupled-cluster theory. Then the inclusion of approximate triples to the correlation energy is explained and illustrated. Section IV is a condensed description of the perturbed coupled-cluster theory and provide details of how to incorporate the effects of an additional perturbation to the residual Coulomb interaction in atomic systems. Results are presented and discussed in Sec. V. In the paper, all the calculations and mathematical expressions are in atomic units ($e=\hbar=m_e=1$).

II. CORRELATION ENERGY FROM MBPT

In this section, to illustrate the stages of our calculations and compare with coupled-cluster theory, we provide a brief description of many-body perturbation theory. Detailed and complete exposition of the method, in the context of atomic many-body theory, can be found in Ref. [19].

The Dirac-Coulomb Hamiltonian H^{DC} is an appropriate choice to incorporate relativistic effects in atoms. This is particularly true for heavy atoms, where the relativistic effects are large for the inner core electrons due to the high nuclear charge. For an N electron atom

$$H^{\mathrm{DC}} = \sum_{i=1}^{N} [c\boldsymbol{\alpha}_i \cdot \boldsymbol{p}_i + (\beta - 1)c^2 - V_N(r_i)] + \sum_{i<j} \frac{1}{r_{ij}}, \quad (1)$$

where α_i and β are the Dirac matrices. For the nuclear potential $V_N(r)$, we consider the finite size Fermi density distribution

$$\rho_{\mathrm{nuc}}(r) = \frac{\rho_0}{1 + e^{(r-c)/a}}, \quad (2)$$

here, $a = t4 \ln 3$. The parameter c is the half-charge radius, that is $\rho_{\mathrm{nuc}}(c) = \rho_0/2$ and t is the skin thickness. The eigen states of H^{DC} are $|\Psi_i\rangle$, the correlated many-particle states with eigenvalues E_i. The eigenvalue equation is

$$H^{\mathrm{DC}}|\Psi_i\rangle = E_i|\Psi_i\rangle. \quad (3)$$

It is however impossible to solve this equation exactly due to the relative coordinates in the electron-electron Coulomb interaction. MBPT is one approach which, starting from a mean-field approximation, incorporates the electron correlation effects systematically.

The starting point of perturbative scheme in MBPT is to split the Hamiltonian as

$$H^{\mathrm{DC}} = H_0 + V, \quad (4)$$

where $H_0 = \Sigma_i[c\boldsymbol{\alpha}_i \cdot \boldsymbol{p}_i + (\beta_i - 1)c^2 - V_N(\boldsymbol{r}_i) + u(\boldsymbol{r}_i)]$, is the unperturbed or zeroth order Hamiltonian. It is the exactly solvable part of the total Hamiltonian and correspond to independent particle model. The average field of the other electrons is the Dirac-Fock central potential $u(\boldsymbol{r}_i)$. The remaining part of the electron-electron Coulomb interaction $V = \Sigma_{i<j}^{N} \frac{1}{r_{ij}} - \Sigma_i u(\boldsymbol{r}_i)$, is the residual Coulomb interaction. The purpose of any atomic many-body theory is to account for this part as accurately as possible. The Hamiltonian H_0 satisfies the eigenvalue equation

$$H_0|\Phi_i\rangle = E_i^0|\Phi_i\rangle, \quad (5)$$

where $|\Phi_i\rangle$ is a many-particle state and E_i^0 is the eigenvalue. The eigenstates are generally Slater determinants, antisymmetrized direct product of single particle states and E_i^0 is the sum of the single particle energies. The difference between the exact and mean field energy, $\Delta E_i = E_i - E_i^0$, is the correlation energy of the i^{th} state. At the single particle level, the relativistic spin orbitals are of the form

$$\psi_{n\kappa m}(\boldsymbol{r}) = \frac{1}{r}\begin{pmatrix} P_{n\kappa}(r)\chi_{\kappa m}(\boldsymbol{r}/r) \\ iQ_{n\kappa}(r)\chi_{-\kappa m}(\boldsymbol{r}/r) \end{pmatrix}, \quad (6)$$

where $P_{n\kappa}(r)$ and $Q_{n\kappa}(r)$ are the large and small component radial wave functions, κ is the relativistic total angular momentum quantum number and $\chi_{\kappa m}(\boldsymbol{r}/r)$ are the spin or spherical harmonics. One representation of the radial components is to define these as linear combination of Gaussian-like functions and are referred to as Gaussian type orbitals (GTOs). Then, the large and small components [20,21] are

$$P_{n\kappa}(r) = \sum_p C_{\kappa p}^L g_{\kappa p}^L(r),$$

$$Q_{n\kappa}(r) = \sum_p C_{\kappa p}^S g_{\kappa p}^S(r). \quad (7)$$

The index p varies over the number of the basis functions. For large component we choose

$$g_{\kappa p}^L(r) = C_{\kappa i}^L r^{n_\kappa} e^{-\alpha_p r^2}, \quad (8)$$

here n_κ is an integer. Similarly, the small component are derived from the large components using kinetic balance condition. The exponents in the above expression follow the general relation

$$\alpha_p = \alpha_0 \beta^{p-1}. \quad (9)$$

The parameters α_0 and β are optimized for an atom to provide good description of the atomic properties. In our case the optimization is to reproduce the numerical result of the total and orbital energies. Besides GTO, B splines is another class of basis functions widely used in relativistic atomic many-body calculations [22]. A description of B splines with details of implementation and examples are given in Ref. [23]. The other important types of basis used in atomic calculations are finite discrete spectrum [24], Slater type orbitals [25] and r multiplied virtuals [26].

The next step in perturbative calculations is to divide the entire Hilbert space of H_0 into two manifolds: model and complementary spaces P and Q, respectively. The model space has, in single reference calculation, the eigenstate $|\Phi_i\rangle$ of H_0 which is a good approximation of the exact eigenstate $|\Psi_i\rangle$ to be calculated. The other eigenstates constitute the complementary space. The corresponding projection operators are

$$P = |\Phi_i\rangle\langle\Phi_i|, \quad Q = \sum_{|\Phi_j\rangle \notin P} |\Phi_j\rangle\langle\Phi_j|, \quad (10)$$

and $P + Q = 1$. In the present paper, we restrict to calculating the ground state $|\Psi_0\rangle$ of the closed-shell inert gas atoms. From here on, for a consistent description, the model space consist of $|\Phi_0\rangle$.

The most crucial part of perturbation theory is to define a wave operator Ω which operates on $|\Phi_0\rangle$ and transform it to $|\Psi_0\rangle$ as

$$|\Psi_0\rangle = \Omega|\Phi_0\rangle. \quad (11)$$

Then, with the intermediate normalization approximation $\langle\Psi_0|\Phi_0\rangle = 1$, the wave operator is evaluated in orders of the perturbation as $\Omega = \Sigma_{i=0}^{\infty}\Omega^{(i)}$ with $\Omega^{(0)} = 1$. It is possible to evaluate $\Omega^{(i)}$ iteratively or recursively from the Bloch equation

$$[\Omega, H_0]P = QV\Omega P - \chi PV\Omega P, \quad (12)$$

where $\chi = \Sigma_{i=1}^{\infty}\Omega^{(i)}$ is the correlation operator. For simplification, in the normal form the perturbation is separated as [19] $V = V_0 + V_1 + V_2$. These are zero-, one- and two-body operators. From these definitions, the first-order wave operator can be separated as

$$\Omega^{(1)} = \Omega_1^{(1)} + \Omega_2^{(1)}. \quad (13)$$

Here, $\Omega_1^{(1)}$ and $\Omega_2^{(1)}$ are one- and two-body components of the first-order wave operator. We obtain singly (doubly) ex-

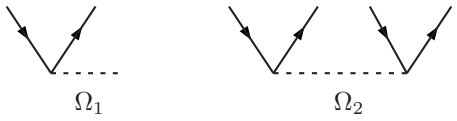

FIG. 1. The diagrammatic representations of the one- and two-body wave operator. Lines with downward (upward) arrows represent core (virtual) single particle states.

cited states $|\Phi_a^p\rangle(|\Phi_{ab}^{pq}\rangle)$ when $\Omega_1^{(1)}(\Omega_2^{(1)})$ operates on the reference state $|\Phi_0\rangle$. The complexity of the expressions increases with order of perturbation and is hard to manage. One powerful tool in many-body perturbation theory is the diagrammatic evaluation of the perturbation expansion. The diagrammatic representation of the $\Omega_1^{(1)}$ and $\Omega_2^{(1)}$ are shown in Fig. 1. Then, the tedious algebraic evaluations are reduced to a sequence of diagrams and equivalent algebraic expressions are derived with simple rules. Even with this approach, it is computationally not practical to go beyond fourth order.

Second- and third-order correlation energy

The ground-state correlation energy ΔE_0, in MBPT, is the sum total of the energy corrections from all orders in perturbation. At the n^{th} order, the energy correction $E_{\text{corr}}^{(n)} = \langle\Phi_0|V\Omega^{(n-1)}|\Phi_0\rangle$ and $\Delta E_0 = \Sigma_n E_{\text{corr}}^{(n)}$. Then the second-order correlation energy is

$$E_{\text{corr}}^{(2)} = \langle\Phi_0|(V_1 + V_2)(\Omega_1^{(1)} + \Omega_2^{(1)})|\Phi_0\rangle. \tag{14}$$

When Dirac-Fock orbitals are used, the diagonal matrix elements of V_1 are the orbital energies and off diagonal matrix elements are zero. For this reason, it does not contribute to the second-order energy. Then, the second-order correlation energy is

$$E_{\text{corr}}^{(2)} = \langle\Phi_0|V_2\Omega_2^{(1)}|\Phi_0\rangle. \tag{15}$$

The singles are nonzero starting from the second order when Dirac-Fock orbitals are used. And, the triples and quadruples also begin to contribute from this order. The triples consist of connected diagrams, whereas all the quadruples are disconnected. The third-order correlation energy is

$$E_{\text{corr}}^{(3)} = \langle\Phi_0|(V_1 + V_2)(\Omega_1^{(2)} + \Omega_2^{(2)} + \Omega_3^{(2)} + \Omega_4^{(2)})|\Phi_0\rangle. \tag{16}$$

The triple and quadruple excitations do not contribute as V at the most can contract with double excitations. For the same reason mentioned earlier, in second order, V_1 also does not contribute. Then the third-order correlation energy is simplified to

$$E_{\text{corr}}^{(3)} = \langle\Phi_0|\ V_2\Omega_2^{(2)})|\Phi_0\rangle. \tag{17}$$

This is similar in form to the second-order correlation energy. In general, the n^{th} order correlation energy has nonzero contribution from the term $V_2\Omega_2^{(n-1)}$ only. It must be mentioned that the connected triples begin to contribute from the fourth-order energy. This is utilized in perturbative inclusion of triples, in later sections of the paper, while discussing coupled-cluster calculations.

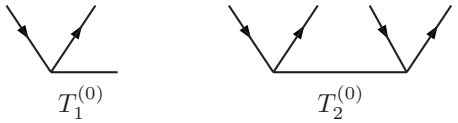

FIG. 2. Diagrammatic representation of unperturbed single and double cluster operators.

III. COUPLED-CLUSTER THEORY

The coupled-cluster theory is a nonperturbative many-body theory and considered as one of the best. A recent review [27] provides an excellent overview of recent developments and different variations. In the context of diagrammatic analysis of MBPT, coupled-cluster theory is equivalent to a selective evaluation of the connected diagrams to all orders. In coupled-cluster theory, for a closed-shell atom, the exact ground state is

$$|\Psi_0\rangle = e^{T^{(0)}}|\Phi_0\rangle, \tag{18}$$

where $T^{(0)}$ is the cluster operator. The superscript is a tag to identify cluster operators arising from different perturbations. For the case of N electron atoms, the cluster operator is

$$T^{(0)} = \sum_{i=1}^{N} T_i^{(0)}. \tag{19}$$

In closed-shell atoms, the single and doubles provide a good approximation of the exact ground state. Then, the cluster operator $T^{(0)} = T_1^{(0)} + T_2^{(0)}$ and is referred to as the coupled-cluster single and doubles (Fig. 2). The cluster operators in the second quantized notations are

$$T_1^{(0)} = \sum_{a,p} t_a^p a_p^\dagger a_a, \tag{20}$$

$$T_2^{(0)} = \frac{1}{2!}\sum_{a,b,p,q} t_{ab}^{pq} a_p^\dagger a_q^\dagger a_b a_a. \tag{21}$$

Here, t_a^p and t_{ab}^{pq} are the single and double cluster amplitudes, respectively, and $ab(pq)$ denote core(virtual) orbitals. Subtracting $\langle\Phi_0|H|\Phi_0\rangle$ from both sides of Eq. (3) and using the normal form of an operator, $O_N = O - \langle\Phi_0|O|\Phi_0\rangle$, we get

$$H_{\text{N}}|\Psi_0\rangle = \Delta E|\Psi_0\rangle, \tag{22}$$

where $\Delta E = E - \langle\Phi_0|H|\Phi_0\rangle$, as defined earlier, is the correlation energy. Operating with $e^{-T^{(0)}}$ and projecting the above equation on excited states we get the cluster amplitude equations

$$\langle\Phi_a^p|\bar{H}_{\text{N}}|\Phi_0\rangle = 0, \tag{23}$$

$$\langle\Phi_{ab}^{pq}|\bar{H}_{\text{N}}|\Phi_0\rangle = 0, \tag{24}$$

where $\bar{H}_{\text{N}} = e^{-T^{(0)}} H_{\text{N}} e^{T^{(0)}}$ is the similarity transformed or dressed Hamiltonian. Following Wick's theorem and structure of H_{N}, in general

$$\overline{H}_{\mathrm{N}} = H_{\mathrm{N}} + \{\overbrace{H_{\mathrm{N}}T^{(0)}}\} + \frac{1}{2!}\{\overbrace{H_{\mathrm{N}}T^{(0)}T^{(0)}}\} + \frac{1}{3!}\{\overbrace{H_{\mathrm{N}}T^{(0)}T^{(0)}T^{(0)}}\} + \frac{1}{4!}\{\overbrace{H_{\mathrm{N}}T^{(0)}T^{(0)}T^{(0)}T^{(0)}}\}, \tag{25}$$

Here

$$\overbrace{A\ldots B}$$

denote contraction between two operators A and B. The single and double cluster amplitudes are solutions of Eqs. (23) and (24), respectively. These are set of coupled nonlinear equations and iterative methods are the ideal choice to solve these equations.

A. Linearized coupled-cluster

The nonlinearity in the cluster amplitude equation arises from the two and higher contractions in the dressed Hamiltonian. An approximation often used as a starting point of coupled-cluster calculations is to retain only the first two terms in $\bar{H}_N$, then

$$\overline{H}_{\mathrm{N}} = H_{\mathrm{N}} + \{\overbrace{H_{\mathrm{N}}T^{(0)}}\}. \tag{26}$$

In the CCSD approximation $T^{(0)}=T_1^{(0)}+T_2^{(0)}$, the cluster equations are

$$\begin{aligned}\langle\Phi_a^p|\{\overbrace{H_{\mathrm{N}}T_1^{(0)}}\} + \{\overbrace{H_{\mathrm{N}}T_2^{(0)}}\}|\Phi_0\rangle &= -\langle\Phi_a^p|H_{\mathrm{N}}|\Phi_0\rangle \\ \langle\Phi_{ab}^{pq}|\{\overbrace{H_{\mathrm{N}}T_1^{(0)}}\} + \{\overbrace{H_{\mathrm{N}}T_2^{(0)}}\}|\Phi_0\rangle &= -\langle\Phi_{ab}^{pq}|H_{\mathrm{N}}|\Phi_0\rangle.\end{aligned} \tag{27}$$

These are the linearized coupled-cluster equations of single and double cluster amplitudes. This can be combined as the matrix equation

$$\begin{pmatrix} H_{11} & H_{12} \\ H_{21} & H_{22} \end{pmatrix}\begin{pmatrix} t_1 \\ t_2 \end{pmatrix} = -\begin{pmatrix} H_{10} \\ H_{20} \end{pmatrix}, \tag{28}$$

where $H_{11}=\langle\Phi_a^p|H_{\mathrm{N}}|\Phi_b^s\rangle$, $H_{12}=\langle\Phi_a^p|H_{\mathrm{N}}|\Phi_{bc}^{st}\rangle$ and so on. The equations are set of coupled linear equations and solved using standard or specialized linear algebra solvers. In the literature several authors refer to linearized coupled-cluster as all-order method. A description of the all-order method and applications are given in Ref. [28]. In a recent work, the authors report the combination of all-order method and configuration interaction [29].

B. Correlation energy and approximate triples

From Eq. (22) the ground-state correlation energy, in coupled-cluster theory

$$\Delta E = \langle\Phi_0|\bar{H}_{\mathrm{N}}|\Phi_0\rangle. \tag{29}$$

The diagrams arising from the above expression are shown in the Fig. 3. The dominant contributions are from the diagrams (a) and (b), which is natural as the doubles cluster amplitudes are larger in value than the singles. Diagram (e) does not contribute to the correlation energy when Dirac-Fock orbitals are used.

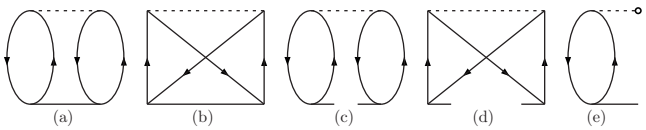

FIG. 3. Coupled-cluster correlation energy diagrams. The diagram (e) is equal to zero when Dirac-Fock orbitals are used.

To go beyond the CCSD approximation, we incorporate selected correlation energy diagrams arising from approximate triples. The approximate triples are perturbative contraction of V_2 with the $T^{(0)}$ cluster amplitudes [30,31]. Example diagrams of the approximate triples and correlation energies are shown in Fig. 4. There are two categories of triples, first is V_2 contracted with $T^{(0)}$ through a hole line, and second contraction through a particle line [Fig. 4(a)]. To calculate the correlation energy from the triples, these are contracted perturbatively with V_2 and reduced to a double excitation diagram. Then the correlation energy is obtained after another contraction with V_2. These two contractions generate several diagrams. The triples correlation energy diagrams are separated into three categories based on the number of internal lines. These are: two particle and two hole internal lines (2p-2h), three particle one hole internal lines (3p-1h), and one particle three hole internal lines (1p-3h). In the present calculations eight diagrams from the first category and two each from other remaining two categories are considered.

IV. PERTURBED COUPLED-CLUSTER

The atomic properties of interest are, in general, associated with additional interactions. The interaction are either internal such as hyperfine interaction or external such as static electric field. These are treated as perturbations which modify the wave function and energy of the atom. This section briefly describes a method to incorporate an additional perturbation within the frame work of relativistic coupled-cluster. The scheme is referred to as perturbed coupled-cluster theory. It has been tried and tested in precision atomic properties and structure calculations. In the presence of a perturbation H_1, the eigen value equation is

$$(H^{\mathrm{DC}} + \lambda H_1)|\tilde{\Psi}_0\rangle = \tilde{E}|\tilde{\Psi}_0\rangle. \tag{30}$$

Here $|\tilde{\Psi}_0\rangle$ is the perturbed wave function, $\tilde{E}$ is the corresponding eigenvalue and λ is the perturbation parameter. The perturbed wave function is the sum of the unperturbed wave function and a correction $|\bar{\Psi}_0^1\rangle$ arising from H_1. That is

$$|\tilde{\Psi}_0\rangle = |\Psi_0\rangle + \lambda|\bar{\Psi}_0^1\rangle. \tag{31}$$

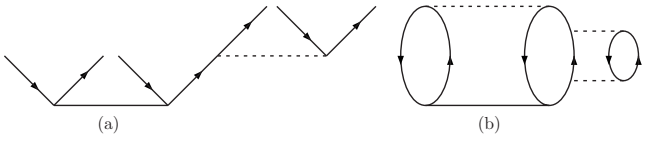

FIG. 4. Diagrams of approximate triples calculated perturbatively: (a) approximate triples cluster operator and (b) correlation energy arising from approximate triples.

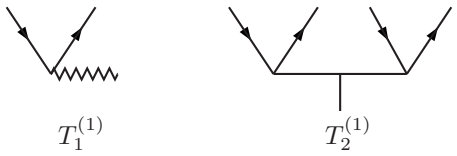

FIG. 5. Diagrams of single and double perturbed cluster operators.

Following the earlier description of coupled-cluster wave function, the perturbed wave function is

$$|\tilde{\Psi}_0\rangle = e^{T^{(0)}+\lambda T^{(1)}}|\Phi_0\rangle. \tag{32}$$

The cluster operators $T^{(0)}$, as defined earlier, incorporate the effects of residual Coulomb interaction. For clarity these are referred as unperturbed cluster operator. The $T^{(1)}$ cluster operators arise from H_1 and are referred to as the perturbed cluster operators (Fig. 5). It acts on the reference state $|\Phi_0\rangle$ to generate the correction. Consider the perturbation expansion to first order in λ, we get

$$|\tilde{\Psi}_0\rangle = e^{T^{(0)}}(1+\lambda T^{(1)})|\Phi_0\rangle. \tag{33}$$

To derive the cluster equations use this in Eq. (30), then operate with $e^{-T^{(0)}}$ and project on excited states. We get the equations for singles and doubles perturbed cluster amplitudes

$$\langle\Phi_a^p|\{\overline{\overline{H_N}T^{(1)}}\}|\Phi_0\rangle = -\langle\Phi_a^p|\bar{H}_1|\Phi_0\rangle, \tag{34}$$

$$\langle\Phi_{ab}^{pq}|\{\overline{\overline{H_N}T^{(1)}}\}|\Phi_0\rangle = -\langle\Phi_{ab}^{pq}|\overline{H}_1|\Phi_0\rangle. \tag{35}$$

The dressed Hamiltonian $\bar{H}_N$ is same as in Eq. (25). Like in linearized coupled-cluster, these form a set of linear algebraic equations.

A. Approximate triples

Like in $T^{(0)}$, a perturbed triple cluster Fig. 6(a) is a perturbative contraction between V_2 and $T_2^{(1)}$. As in the case of unperturbed approximate triples discussed earlier, there are two types of diagrams in the present case as well. One arises from particle line contraction and the other from hole line contraction between V_2 and $T^{(1)}$ diagrams. In this work we implement approximate triples while calculating properties.

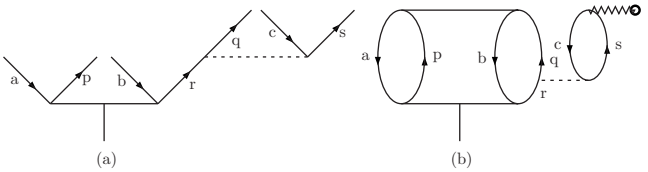

FIG. 6. Diagrams of approximate triples calculated perturbatively: (a) representation of approximate perturbed triples. (b) Contribution of approximate perturbed triples to the dipole polarizability.

In particular, to calculate dipole polarizability and an example diagram is shown in Fig. 6(b). The algebraic expression of this diagram is

$$\sum_{a,b,c,p,q,r,s} \frac{\langle ab|T_2^{(0)\dagger}|pq\rangle\langle c|\boldsymbol{d}|s\rangle\langle qs|V_2|rc\rangle\langle pr|T_2^{(1)}|ab\rangle}{\epsilon_a+\epsilon_b+\epsilon_c-\epsilon_p-\epsilon_q-\epsilon_s}, \tag{36}$$

here, $\boldsymbol{d}$ is the dipole operator. In total there are twentyfour properties diagrams arising from the perturbative triples and we include all of these diagrams in the calculations.

B. Dipole polarizability

When an atom is placed in an external electric field $\mathcal{E}$, the charge distribution of electron cloud is distorted and an electric dipole moment $\boldsymbol{D}_{\rm ind}$ is induced. The dipole polarizability of the atom α is then the ratio of the induced dipole moment to the applied electric field, that is

$$\boldsymbol{D}_{\rm ind} = \alpha\mathcal{E}. \tag{37}$$

By definition, the dipole polarizability of the ground state is

$$\alpha = -2\sum_I \frac{|\langle\Psi_0|\boldsymbol{D}|\Psi_I\rangle|^2}{E_0-E_I}, \tag{38}$$

where $|\Psi_I\rangle$ are intermediate atomic states. These are opposite in parity to the ground state $|\Psi_0\rangle$. The expression of α can be rewritten as

$$\alpha = -2\langle\Psi_0|\boldsymbol{D}|\bar{\Psi}_0^1\rangle. \tag{39}$$

Here $|\bar{\Psi}_0^1\rangle = \Sigma_I(|\Psi_I\rangle\langle\Psi_I|\boldsymbol{D}|\Psi_0\rangle)/(E_0-E_I)$, which follows from the first-order time independent perturbation theory. The perturbation Hamiltonian is $H_1 = -\boldsymbol{D}\cdot\mathcal{E}$ and external field $\mathcal{E}$ is the perturbation parameter. One short coming of calculating α from Eq. (38) is, for practical reasons, the summation over I is limited to the most dominant intermediate states. However, the summation is avoided altogether when the perturbed coupled-cluster wave functions are used in the calculations. From Eq. (32) the perturbed wave function

$$|\bar{\Psi}_0^1\rangle = e^{T^{(0)}}T^{(1)}|\Phi_0\rangle. \tag{40}$$

In a more compact form, the dipole polarizability in terms of the perturbed coupled-cluster wave function is

$$\alpha = \langle\tilde{\Psi}_0|\boldsymbol{D}|\tilde{\Psi}_0\rangle. \tag{41}$$

After simplification, using the perturbed wave function in Eq. (32), we get

$$\alpha = \langle\bar{\Psi}_0^1|\boldsymbol{D}|\Psi_0\rangle + \langle\Psi_0|\boldsymbol{D}|\bar{\Psi}_0^1\rangle. \tag{42}$$

The correction $|\bar{\Psi}_0^1\rangle$, as described earlier, is opposite in parity to $|\Phi_0\rangle$. Hence the matrix elements $\langle\Psi_0|\boldsymbol{D}|\Psi_0\rangle$ and $\langle\bar{\Psi}_0^1|\boldsymbol{D}|\bar{\Psi}_0^1\rangle$ are zero. As D is Hermitian, the two terms on the left-hand side are identical and the above expression is same as Eq. (39). Considering the leading terms

TABLE I. Values of the parameters, α and β, used in the calculations, and p is the number of basis functions.

	Ne			Ar			Kr			Xe		
Symmetry	α	β	p	α	β	p	α	β	p	α	β	p
s	0.0925	1.4500	38	0.0985	1.8900	38	0.0002	2.0220	30	0.0001	2.0220	32
p	0.1951	2.7103	35	0.0072	2.9650	35	0.0072	2.3650	28	0.0072	2.3650	28
d	0.0070	2.7000	25	0.0070	2.7000	28	0.0070	2.5500	25	0.0070	2.5500	25

$$\alpha = \langle \Phi_0 | T^{(1)\dagger} \bar{D}^{(0)} + \bar{D}^{(0)} T^{(1)} | \Phi_0 \rangle. \quad (43)$$

Here, the operator $\bar{D}^{(0)} = e^{T^{(0)\dagger}} D e^{T^{(0)}}$ is the unitary transformed electric dipole operator. It is explicitly evident that the dipole polarizability, in terms of perturbed cluster operator, does not have a sum over states. In this scheme, contributions from all intermediate states within the chosen configuration space are included. For precision calculations, this is a very important advantage.

V. RESULTS

In order to get reliable results, in atomic structure and properties calculations, one prerequisite is good quality orbital basis set. In all calculations described in the paper, we employ GTOs as orbital functions. In particular, we use even tempered basis in which the parameters α_0 and β, in Eq. (9), are different for each symmetries. We use the basis parameters of Tatewaki and Watanabe [32] as starting values and optimized further to obtain $E_{\mathrm{DC}}^{(0)}$ (ground state Dirac-Fock energy) and ϵ_a (single particle energies of core orbitals) in agreement with the numerical results. The values of α and β chosen for the occupied symmetries are given in Table I. For the symmetries which occur only as virtual orbitals we chose the optimal values of 0.0070 and 2.6950 for α and β, respectively. The numerical results are obtained from the GRASP92 [33] code. In order to obtain converged $E_{\mathrm{corr}}^{(2)}$, we consider orbital basis set consisting of all the core orbitals and virtual orbitals up to 10 000–11 000 in single particle energies.

The working equations of coupled-cluster theory are coupled nonlinear equations. Solving these equations is a computational challenge. The number of unknowns, cluster amplitudes, are in the order of millions. In addition, implementing fast and efficient algorithms demand huge memory to tabulate and store two-electron integrals. This is essential as the two-electron integrals are needed repeatedly and are compute intensive. For the larger basis sets in the present work, the number of two-electron integrals exceed 2×10^8. In order to utilize memory efficiently, we have developed a scheme which parallelize the tabulation and storage of two-electron integrals.

The unperturbed and perturbed cluster amplitude equations are solved iteratively using Jacobi method. We chose the method as it is relatively simple to parallelize. However, one drawback of the method is slow convergence. To obtain faster convergence, we employ direct inversion in iterated subspace (DIIS) [34] convergence acceleration.

A. Second-order correlation energy

The SCF energy $E_{\mathrm{DC}}^{(0)}$, second-order correlation energy $E_{\mathrm{corr}}^{(2)}$ and the total energy E from our calculations are listed in Table II. For comparison the results of previous calculations are also listed. It is evident that our second-order correlation energy and total energy, sum of the SCF and second-order correlation energy, are in agreement with the results of Ishikawa *et al.* [35] for all the atoms studied. The results in the table other than [35] are from nonrelativistic calculations. For all the atoms, our SCF energy E_{DC}^{0} are lower and there are no discernible trends, as a function of nuclear charge, in the difference. Interestingly, except for Xe, our second-order correlation energies are higher. This compensates the lower $E_{\mathrm{DC}}^{(0)}$ and subsequently, the total energies E of the two calculations are in excellent agreement.

The Table III lists the cumulative contributions from various symmetries to $E_{\mathrm{corr}}^{(2)}$. Among the previous works, Lindgren and collaborators [36] provide cumulative $E_{\mathrm{corr}}^{(2)}$ for Ne up to i symmetry. Their converged result, with orbitals up to i symmetry, is −0.3836. However, in our calculation, we get converged results of −0.3830 after including j and k symmetry orbitals. The contribution from k symmetry to $E_{\mathrm{corr}}^{(2)}$ for Ar, Kr, and Xe are −0.0017, −0.0083, and −0.0176 respectively. These are larger than that of Ne, which is −0.0007. However, these correspond to 0.24%, 0.45% and 0.59% for Ar, Kr and Xe, respectively, these compare very well with that of Ne 0.20%. For Ar there is a variation in the previous values of $E_{\mathrm{corr}}^{(2)}$, these range from the lowest value of Clementi [37] −0.790 to that of Ishikawa [35] −0.6981. Our value of −0.6938 is closer to that of Ishikawa.

There is a pattern in the change of the correlation energy with symmetry wise augmentation, without changing α and β, of the virtual orbital set. There is an initial increase, reaches a maximum and then decreases. The maximum change occurs with the addition of p, d, d, and f symmetry for Ne, Ar, Kr, and Xe, respectively. The pattern is evident in Fig. 7, which plots the change in $E_{\mathrm{corr}}^{(2)}$ with symmetry wise augmentation of the virtual space. The pattern arise from the distribution of the contributions from each of the core orbitals. Extrapolating the results to $l \to \infty$, $E_{\mathrm{corr}}^{(2)}$ are −0.3838, −0.6966, −1.8549 and −2.9969 for Ne, Ar, Kr, and Xe, respectively. Depending on the core orbital combination ab, there are two types of correlation effects. These are inter- and intracore shell correlations corresponding to $a=b$ and $a \neq b$, respectively. Among the various combinations, the $2p_{3/2}2p_{3/2}$, $3p_{3/2}3p_{3/2}$, $3d_{5/2}3d_{5/2}$, and $4d_{5/2}4d_{5/2}$ core orbital pairings have leading contributions in Ne, Ar, Kr, and Xe, respectively. Here for Ne and Ar the leading pairs correspond

TABLE II. The SCF $E_{DC}^{(0)}$, the second-order correlation $E_{corr}^{(2)}$ and the total energies E of Ne, Ar, Kr and Xe. All the values listed are in atomic units (hartrees).

			This work			Other work		
Atom	Z	Atomic mass	$E_{DC}^{(0)}$	$E_{corr}^{(2)}$	E	$E_{DC}^{(0)}$	$E_{corr}^{(2)}$	E
Ne	10	20.18	−128.6932	−0.3830	−129.0762	−128.6919	−0.3834[a]	−129.0753
							−0.3836[b]	
							−0.3822[c]	
							−0.3697[d]	
							−0.3804[e]	
Ar	18	39.95	−528.6882	−0.6938	−529.3820	−528.6838	−0.6981[a]	−529.3819
							−0.6822[e]	
							−0.685 [f]	
							−0.790 [g]	
Kr	36	83.80	−2788.8659	−1.8426	−2790.7085	−2788.8615	−1.8468[a]	−2790.7083
Xe	54	131.29	−7446.8887	−2.9767	−7449.8654	−7446.8880	−2.9587[a]	−7449.8467

[a]Reference [35].
[b]Reference [36].
[c]Reference [38].
[d]Reference [39].
[e]Reference [40].
[f]Reference [41].
[g]Reference [37].

to the valence shell but it is the last d shell for Kr and Xe. This correlates with the pattern observed in the symmetry wise augmentation.

B. Third-order correlation energy

We calculate the third-order correlation energy $E_{corr}^{(3)}$ from the linearized CCSD equations. This is possible when the first-order MBPT wave operator $\Omega^{(1)}$ is chosen as the initial guess and iterate the linearized coupled-cluster equations once. The two-body wave operator so obtained is $\Omega_2^{(2)}$ and from Eq. (17) $E_{corr}^{(3)}=\langle\Phi_0|V_2\Omega_2^{(2)}|\Phi_0\rangle$. This approach, however, is not applicable beyond third order. The reason is, starting from the fourth order correlation energy the triples contribute to ΔE_0 and triples are not part of the linearized CCSD equations. The results of $E_{corr}^{(3)}$, obtained from our calculations, are listed in Table IV. For comparison, results from previous works are also listed. For Ne, Jankowski and Malinowski [42] reported a value of 0.0024. Their calculations were done with a limited basis set and hence, could leave out less significant contributions. The results of Lindgren and collaborators [36] 0.0035 is perhaps more accurate and reliable on account of larger basis set. In our calculations, we include virtual orbitals up to i symmetry, then extrapolate up to k symmetry based on $E_{corr}^{(2)}$ results. We obtain 0.0019, which is in better agreement with the result of Jankowski and Malinowski [42]. As expected, $E_{corr}^{(3)}$ increases with Z and to our knowledge, our results of Ar, Kr, and Xe are the first reported calculations in literature. Interestingly, $E_{corr}^{(3)}$ is positive for Ne, Kr, and Xe but it is negative for Ar.

TABLE III. Cumulative second-order correlation energy when orbitals up to a particular symmetry are included in the virtual space. All the values are in atomic units.

Symmetry	Ne	Ar	Kr	Xe
s	−0.0194	−0.0210	−0.0236	−0.0247
p	−0.1920	−0.2043	−0.2479	−0.2687
d	−0.3216	−0.5401	−0.9512	−1.0419
f	−0.3589	−0.6330	−1.5213	−2.2972
g	−0.3732	−0.6695	−1.7077	−2.6879
h	−0.3786	−0.6830	−1.7843	−2.8520
i	−0.3811	−0.6891	−1.8179	−2.9238
j	−0.3823	−0.6921	−1.8343	−2.9591
k	−0.3830	−0.6938	−1.8426	−2.9767

C. Coupled-cluster correlation energy

The MBPT correlation energies $E_{corr}^{(i)}$ converges with relatively large basis set. For example, the $E_{corr}^{(2)}$ of Ne converge

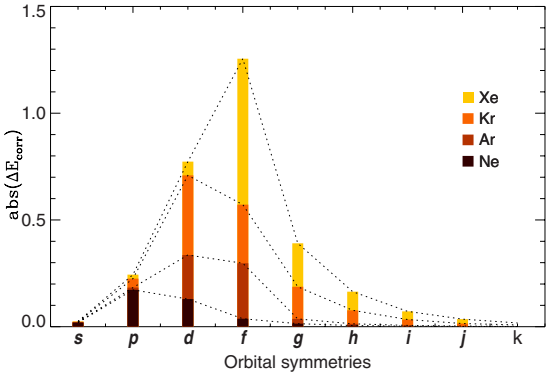

FIG. 7. (Color online) The second-order energy (in Hartrees) when orbitals up to a particular symmetry are included in the virtual space.

TABLE IV. Third-order correlation energy in atomic units.

	E_3	
Atom	This work	Other work
Ne	0.0019	0.0035[a]
		0.0024[b]
Ar	−0.0127	
Kr	0.0789	
Xe	0.1526	

[a]Reference [36].
[b]Reference [42].

when virtual orbitals up to k symmetry are included in the calculations. This correspond to a total of 224 virtual orbitals. Similar or larger number of virtual orbitals are required to obtain converged $E_{\mathrm{corr}}^{(2)}$ of Ar, Kr, and Xe as well. However, it is not practical to have such large basis sets in relativistic coupled-cluster calculations. The $n_v^4 n_c^3$, where n_v and n_c are the number of the virtual and core orbitals, respectively, scaling of arithmetic operations in CCSD render computations with large n_v beyond the scope of detailed studies. Hence, in the CCSD calculations, the size of the virtual orbital set is reduced to a manageable level and restrict up to the h symmetry. To choose the optimal set, after considering the most dominant ones, the virtual orbitals are augmented in layers. Where one layer consists of one virtual orbital each from all the symmetries considered.

The CCSD correlation energies for two basis sets are listed in Table V. The first is with a basis set considered optimal and manageable size for CCSD calculations after a series of calculations. Then the next is with an additional layer of virtual orbitals. The change in the linearized CCSD

TABLE V. Correlation energy from coupled-cluster. All the values are in atomic units.

		ΔE (CCSD)	
Atom	Active Orbitals	Linear	Nonlinear
Ne	$17s10p10d9f9g8h$	−0.3783	−0.3760
	$18s11p11d10f10g9h$	−0.3805	−0.3782
	Estimated	−0.3905	−0.3882
Ar	$17s11p11d9f9g9h$	−0.6884	−0.6829
	$18s12p12d10f10g10h$	−0.7001	−0.6945
	Estimated	−0.7258	−0.7202
Kr	$22s13p11d9f9g9h$	−1.5700	−1.5688
	$23s14p12d10f10g10h$	−1.6730	−1.6716
	Estimated	−1.8480	−1.8466
Xe	$23s14p12d10f10g10h$	−2.5500	−2.5509
	$24s15p13d11f11g11h$	−2.6874	−2.6881
	Estimated	−2.9973	−2.9979

TABLE VI. Correlation energy arising from the approximate triples in the coupled-cluster theory. All the values are in atomic units.

		ΔE		
Atom	Basis size	2p-2h	1p-3h	3p-1h
Ne	$18s11p11d10f10g9h$	0.00672	−0.00145	−0.00164
Ar	$18s12p12d10f10g10h$	0.00805	−0.00066	−0.00192
Kr	$22s13p11d9f9g9h$	0.01546	−0.00171	−0.00305
Xe	$19s15p10d9f5g2h$	0.02011	−0.00148	−0.00260

ΔE_0 with the additional layer of virtual orbitals are 0.2%, 1.7%, 6.0% and 5.0% for Ne, Ar, Kr, and Xe, respectively. Changes of similar order are observed in the corresponding ΔE_0 of the nonlinear CCSD calculations. It must be mentioned that, though the difference in ΔE_0 is small, the computational cost of nonlinear CCSD is much higher than the linearized CCSD calculations. The percentage changes indicate the basis size of Kr and Xe are not large enough. The orbital basis of Xe, with the additional layer, consists of 17 core and 129 virtual orbitals. This translates to $\sim 5.0 \times 10^6$ cluster amplitudes, which follows from the $n_v^2 n_c^2$ scaling of the number of cluster amplitudes. At this stage, the computational efforts and costs far out weight the gain in accuracy. To account for the correlation energy from the other virtual orbitals, not included in the CCSD calculations, we resort to the second-order correlation energy. For this we calculate $E_{\mathrm{corr}}^{(2)}$ with the basis set chosen in CCSD calculations and subtract from the converged $E_{\mathrm{corr}}^{(2)}$. The estimated ΔE in Table V is the sum of this difference and CCSD ΔE. This includes the correlation effects from i, j, and k symmetries as well. For Ne, the estimated experimental value of correlation energy lies between the range 0.385 and 0.390 [39,43]. Our coupled-cluster result, estimated value, is in excellent agreement.

The contributions to the correlation energy arising from the approximate triples are listed in Table VI. As discussed in Sec. III B, the correlation energy diagrams corresponding to the approximate triples are grouped into three classes. Out of these we have selected a few: eight from 2p-2h and two each from 3p-1h and 1p-3h. In Table VI, ΔE_0 arising from these are listed. It is evident from the table, the contribution from 1p-3h and 3p-1h are negative and adds to the magnitude of ΔE_0. Whereas, the contribution from 2p-2h is positive and reduces the magnitude of ΔE_0.

D. Dipole polarizability

One constraint while using perturbed coupled-cluster theory to calculate dipole polarizability is the form of $\bar{D}$. It is a unitary transformation of the dipole operator and expands to a nonterminating series. For the present calculations we consider the leading terms in $T^{(1)\dagger}\bar{D}$. That is, we use the approximation

$$T^{(1)\dagger}\bar{D} \approx T_1^{(1)\dagger}[D + DT_1^{(0)} + DT_2^{(0)}] + T_2^{(1)\dagger}[DT_2^{(0)} + DT_1^{(0)}]. \tag{44}$$

The ground state dipole polarizabilities of Ne, Ar, Kr, and Xe calculated with this approximation are given in Table VII.

TABLE VII. Dipole polarizability of the ground state of neutral rare-gas atoms (in a.u.).

Contributions	Ne	Ar	Kr	Xe
$T_1^{(1)\dagger}D$	2.7108	11.3330	17.2115	27.7427
$T_1^{(1)\dagger}DT_1^{(0)}$	0.0771	0.0486	0.0429	−0.1495
$T_1^{(1)\dagger}DT_2^{(0)}$	−0.0703	−0.8264	−1.2721	−2.3286
$T_2^{(1)\dagger}DT_1^{(0)}$	−0.0004	−0.0001	0.0002	0.0027
$T_2^{(1)\dagger}DT_2^{(0)}$	0.0053	0.2490	0.0439	0.0786
Total(CCSD)	2.7225	10.8041	16.0264	25.3459
Approx. triples	2.7281	10.7360	16.0115	25.2974
Expt. values[a]	2.670 ± 0.005	11.070(7)	17.075	27.815

[a]Reference [18].

Among the various terms, the first term $T^{(1)\dagger}D$ subsumes contributions arising from Dirac-Fock and random phase approximation. We can thus expect this term to have the most dominant contribution. This is evident in Table VII, which shows that the contribution from $T^{(1)\dagger}D$ is far larger than the others. The next leading term is $T_1^{(1)\dagger}DT_2^{(0)}$. This is attributed to the larger values, compared to $T_1^{(0)}$, of $T_2^{(0)}$ cluster amplitudes. The dipole polarizability calculations with relativistic coupled-cluster theory involve two sets of cluster amplitudes. These are the $T^{(0)}$ and $T^{(1)}$ cluster amplitudes. As mentioned earlier, solving coupled-cluster equations is compute intensive.

One pattern discernible in the results is the better agreement between the $T^{(1)\dagger}D$ results and experimental data. The deviations from the experimental data are large when we consider the total (CCSD) result. For Ne, the deviation from experimental data is 2%, where as it is 9% in the case of Xe atom. We attribute this to the approximation in Eq. (44) and partly to the basis set. To confirm this, however, requires detailed computations with higher order terms in the unitary transformation. This poses considerable computational challenges and shall be addressed in future publications. We also implement the approximate triples excitation of the perturbed cluster amplitudes and contribution (arising from the twentyfour diagrams) to α are listed in the table.

VI. CONCLUSION

We have done a systematic study of the electron correlation energy of neutral inert gas atoms using relativistic MBPT and coupled-cluster theory. Our MBPT results are based on larger basis sets consisting of higher symmetries than the previous works, and hence more reliable and accurate. Our study shows that in heavier atoms Kr and Xe, the inner core electrons in *d* shells dominates the electron correlation effects. This ought to be considered in high precision properties calculations. For example, the EDM calculations of Xe arising from nuclear Schiff moment. The dipole polarizability calculated with the perturbed coupled-cluster show systematic deviation from the experimental data. However, the contribution from the leading term $T_1^{(1)^\dagger}D$ is in good agreement with the experimental data. The deviations might decrease when higher order terms are incorporated in the properties calculations. From these results, it is evident that the basis set chosen is of good quality and appropriate for precision calculations.

ACKNOWLEDGMENTS

We wish to thank S. Chattopadhyay, S. Gautam, B. Sahoo, and S. A. Silotri for useful discussions. The results presented in the paper are based on computations using the HPC cluster of the Center for computational Material Science, JNCASR, Bangalore.

[1] W. C. Griffith, M. D. Swallows, T. H. Loftus, M. V. Romalis, B. R. Heckel, and E. N. Fortson, Phys. Rev. Lett. **102**, 101601 (2009).
[2] K. Tsigutkin, D. Dounas-Frazer, A. Family, J. E. Stalnaker, V. V. Yashchuk, and D. Budker, Phys. Rev. Lett. **103**, 071601 (2009).
[3] M. A. Rosenberry and T. E. Chupp, Phys. Rev. Lett. **86**, 22 (2001).
[4] V. A. Dzuba, V. V. Flambaum, J. S. M. Ginges, and M. G. Kozlov, Phys. Rev. A **66**, 012111 (2002).
[5] F. Coester, Nucl. Phys. **7**, 421 (1958).
[6] F. Coester and H. Kümmel, Nucl. Phys. **17**, 477 (1960).
[7] G. Hagen, T. Papenbrock, D. J. Dean, and M. Hjorth-Jensen, Phys. Rev. Lett. **101**, 092502 (2008).
[8] H. S. Nataraj, B. K. Sahoo, B. P. Das, and D. Mukherjee, Phys. Rev. Lett. **101**, 033002 (2008).
[9] R. Pal, M. S. Safronova, W. R. Johnson, A. Derevianko, and S. G. Porsev, Phys. Rev. A **75**, 042515 (2007).
[10] T. A. Isaev, A. N. Petrov, N. S. Mosyagin, A. V. Titov, E. Eliav, and U. Kaldor, Phys. Rev. A **69**, 030501(R) (2004).
[11] R. F. Bishop, P. H. Y. Li, D. J. J. Farnell, and C. E. Campbell, Phys. Rev. B **79**, 174405 (2009).
[12] K. V. Latha, D. Angom, B. P. Das, and D. Mukherjee, Phys. Rev. Lett. **103**, 083001 (2009).
[13] L. W. Wansbeek, B. K. Sahoo, R. G. E. Timmermans, K. Jungmann, B. P. Das, and D. Mukherjee, Phys. Rev. A **78**, 050501(R) (2008).
[14] B. K. Sahoo, Phys. Rev. A **80**, 012515 (2009).
[15] C. Thierfelder and P. Schwerdtfeger, Phys. Rev. A **79**, 032512 (2009).
[16] B. K. Sahoo, B. P. Das, and D. Mukherjee, Phys. Rev. A **79**, 052511 (2009).
[17] K. V. Latha, D. Angom, B. P. Das, R. K. Chaudhuri, B. P. Das, and D. Mukherjee, J. Phys. B **41**, 035005 (2008).
[18] U. Hohm and K. Kerl, Mol. Phys. **69**, 803 (1990); **69**, 819 (1990).
[19] I. Lindgren and J. Morrison, in *Atomic Many-Body Theory* (Springer-Verlag, Berlin, 1985).
[20] A. K. Mohanty and E. Clementi, Chem. Phys. Lett. **157**, 348 (1989).

[21] R. K. Chaudhuri, P. K. Panda, and B. P. Das, Phys. Rev. A **59**, 1187 (1999).
[22] W. R. Johnson, S. A. Blundell, and J. Sapirstein, Phys. Rev. A **37**, 307 (1988).
[23] W. R. Johnson, *Atomic Structure Theory: Lectures on Atomic Physics* (Springer Verlag, Berlin, 2007).
[24] S. Salomonson and P. Öster, Phys. Rev. A **40**, 5559 (1989).
[25] J. C. Slater, Phys. Rev. **36**, 57 (1930).
[26] E. L. Shirley and R. M. Martin, Phys. Rev. B **47**, 15404 (1993).
[27] R. J. Bartlett and M. Musial, Rev. Mod. Phys. **79**, 291 (2007).
[28] M. S. Safronova and W. R. Johnson, Adv. At., Mol., Opt. Phys. **55**, 191 (2007).
[29] M. S. Safronova, M. G. Kozlov, W. R. Johnson, and D. Jiang, Phys. Rev. A **80**, 012516 (2009).
[30] K. Raghavachari, G. W. Trucks, J. A. Pople, and M. Head-Gordon, Chem. Phys. Lett. **157**, 479 (1989).
[31] S. G. Porsev and A. Derevianko, Phys. Rev. A **73**, 012501 (2006).
[32] H. Tatewaki and Y. Watanabe, J. Chem. Phys. **121**, 4528 (2004).
[33] F. A. Parpia, C. Froese Fischer, and I. P. Grant, Comput. Phys. Commun. **94**, 249 (1996).
[34] P. Pulay, Chem. Phys. Lett. **73**, 393 (1980).
[35] Y. Ishikawa and K. Koc, Phys. Rev. A **50**, 4733 (1994).
[36] I. Lindgren and S. Salomonson, Phys. Scr. **21**, 335 (1980).
[37] E. Clementi, IBM J. Res. Dev. **9**, 2 (1965).
[38] R. K. Nesbet, Phys. Rev. **175**, 2 (1968).
[39] F. Sasaki and M. Yoshimine, Phys. Rev. A **9**, 17 (1974).
[40] Y. Ishikawa, Phys. Rev. A **42**, 1142 (1990).
[41] E. R. Cooper and H. P. Kelly, Phys. Rev. A **7**, 38 (1973).
[42] K. Jankowski and P. Malinowski, Phys. Rev. A **21**, 45 (1980).
[43] C. F. Bunge and E. M. A. Peixoto, Phys. Rev. A **1**, 1277 (1970).